Int. J. Electrochem. Sci., 15 **(2020)** 11238 – 11249, doi: 10.20964/2020.11.04

International Journal of
ELECTROCHEMICAL
SCIENCE
www.electrochemsci.org

Gold/Copper-Based Metal-Organic Framework/Glassy Carbon Electrode as High Efficient Electrochemical Sensor for Determination of Hydrogen Peroxide

Danfeng He[1], *Fujiang Zhou*[2], *Liqun Sun*[1], *Yanbin Tong*[1], *Long Tang*[1,*], *Zhicheng Zhong*[3], *Hongqin Li*[3]

[1] Heilongjiang Provincial Key Laboratory of Oilfield Applied Chemistry and Technology, Daqing Normal University, Daqing 163712, China
[2] Daqing Oileld Chemical Corporation, Daqing, Heilongjiang, 163712, China
[3]College of Instrumentation and Electrical Engineering, Jilin University, Changchun 130012, China
[*]E-mail: tanglong088@163.com and choubuzhongjiang@163.com

Received: 2 June 2020 / *Accepted:* 23 August 2020 / *Published:* 30 September 2020

In this study, the modified gold/copper-based metal-organic framework on glassy carbon electrodes [(Au_x:Cu_y)-MOFs/GCE (x, y = 0, 1, 2 and 3 as volume ratio)] were applied for electrochemical determination of hydrogen peroxide (H_2O_2). (Au_x:Cu_y)-MOFs were synthesized through the oriented growth method and were applied to modification of GCE. SEM and XRD analyses were employed to structural studies of synthesized (Au_x:Cu_y)-MOFs. Cyclic voltammetry and amperometry techniques were used to electrochemical characterization of (Au_x:Cu_y)-MOFs/GCE as H_2O_2 sensor. Results showed that (Au_x:Cu_y)-MOFs were synthesized in porous and densely packed irregular nano-sheet structure. The electrochemical studies showed that (Au_1:Cu_2)-MOF/GCE was fast response, sensitive, stable and selective sensor for the determination of H_2O_2. The wide linear range, sensitivity and detection limit of the sensor were estimated of 1 to 19 µM, 2.022 µA/ µM and 0.014 µM, respectively. Comparison performance (Au_1:Cu_2)-MOF/GCE with other H_2O_2 sensor exhibits higher or comparative sensitivity in determination of H_2O_2. Study the sensor response to the determination of H_2O_2 in real sample indicated satisfactory RSD and recovery values was less than 4.51% and more than 91.86%, respectively.

Keywords: Hydrogen peroxide; Metal-organic framework; Amperometry technique; Sensitivity and selectivity electrochemical sensor

1. INTRODUCTION

Hydrogen peroxide (H_2O_2) as product of many reactions catalyzed by oxidases [1] and oxidative biosynthetic agent are used in wide range in cosmetics, antiseptic, detergent, dentistry, water purification, and food and drug industries. Its toxicity is not high but skin inflammation and damages have been observed due to expose to cleaner solutions with high concentration of H_2O_2 (> 25%) [2-4]. It has hydroxyl and oxygen-containing free radicals which are able to attack to important body

macromolecules such as cell, DNA, proteins, carbohydrates, and lipids [5]. These radical damages lead to diseases such as inflammatory, cancer, atherosclerosis, and infections [6-8].

Thus, there are some limitation for the application of H_2O_2 in cosmetic, food and pharmacy industries. For example, in the UK, use of H_2O_2 content higher than 0.1% is illegal for non-dentists. Furthermore, selling H_2O_2 concentrations higher than 12% are considered as a criminal offence. Thus, it is required the study and development of identification and measurement methods of H_2O_2 concentrations [9]. In a few decades, the determination of H_2O_2 is carried out through the colorimetry [10], fluorometry [11], spectrophotometry [12], chromatography [13], photoluminescence [14], chemiluminescence [15], titrimetry [16], and electrochemical methods [17-19]. Most of these methods are expensive and complicated and time- consuming. Further studies exhibited that the electrochemical techniques are suitable for the determination of H_2O_2 due to their simplicity, low coast, and relatively excellent sensing characterization such as selectivity, high sensitivity and stability [20].

It is should be considered, the determination of H_2O_2 by electrochemical methods is usually difficult because of its high over potential and slow kinetics of electron transfer in redox reactions. Another advantage of electrochemical techniques is their ability to promote the sensors properties through modification and miniaturization the sensor tools by application of the enzymes, nanostructures, and nanocomposites on electrode surface of sensors [21, 22]. Among the modifications materials, electrochemical sensors based on enzyme-modified electrodes have attracted a lot of attentions [23]. However, these type of modified electrodes are expensive, limited lifetime, instable, and required complicated process to immobilization enzyme on the surface of electrode [24-26]. Therefore, non-enzymatic modified sensors have been also developed. Nanowires, nanoparticles, nanotubes, graphene and metal-organic frameworks (MOFs) are the most applicable nanomaterials which are used for modification the non-enzymatic sensor's surfaces [27-30].

MOFs are porous coordination polymers which fabricated by the coordination of metal ions or clusters bridged by organic ligands or linkers [31-33]. The more attended properties of MOFs structures are high effective surface area, high porosity, high stability, good absorbability and high catalytic activity which make them as a superb materials for sensor modification [34, 35]. Studies revealed optimizing the MOFs structures by Pt, Au, Ag, Cu, Ni, and Zn for enhance the electrical conductivity lead to promote electrochemical signals for redox activity of analytes [36-38]. One of the optimization methods is use of simultaneous of metallic materials for their stability and high electrical conductivity [39-41]. Therefore, in this study, (Au_x: Cu_y)-MOFs/GCE (x, y = 0, 1, 2 and 3) were used for the determination of H_2O_2. First, (Au_x: Cu_y)-MOFs were synthesized and applied for the modification of GCE. Then, the structural properties of synthesized (Au_x: Cu_y)-MOFs were studied by SEM and XRD analyses. Finally, electrochemical techniques were applied for the determination of H_2O_2 concentrations.

2. EXPERIMENTAL

2.1 Fabrication (Au_x: Cu_y)-MOFs/GCE (x, y = 0, 1, 2 and 3)

Prior modification the bare GCE (d= 3 mm, Wuhan Corrtest Instruments Corp., Ltd., China), the GCE surface was polished sequentially by 0.6-4 μm of alumina powder (Kaifeng Datong Refractories

Co., Ltd., China) for 20 minutes on micro-cloth pads wet with double distilled water, respectively. The polished electrode was washed under ultrasonication bath in ethanol solution (99.98%, Xilong Scientific Co., Ltd., China) for 15 minutes, and double distilled water for 5 minutes, respectively. The polished GCE surface was modified by monolayers of carboxylated graphene (XF NANO INC Advanced Material Supplier, China) through dropping 10 µl of dispersed carboxylated graphene on the surface of GCE. Then, the electrode was dried at room temperature.

[(Au_x: Cu_y)-MOFs/GCE (x, y = 0, 1, 2 and 3 as volume ratio)] preparation was performed according to [42]. 1.674 g 1, 3, 5-benzenetricarboxylic acid (> 98%, BTC, Aladdin Chemistry Co., Ltd, China) was solved to 24 ml ethanol. 24 ml of mixture of 0.33 M $HAuCl_4 \cdot 3H_2O$ (99%, J&K Scientific Ltd., China) and 0.33 M Cu $(NO_3)_2 \cdot 3H_2O$ (> 98%, Aladdin Chemistry Co., Ltd, China) aqueous solutions (1: 0, 0: 1 , 1: 1, 2: 1, 1: 2, 3: 1 and 1: 3 in volume ration *V*:*V* as referred Au-MOFs, Cu-MOFs, (Au: Cu)-MOF/GCE, (Au_2: Cu_1)-MOF/GCE, (Au_1: Cu_2)-MOF/GCE, (Au_3: Cu_1)-MOF/GCE, and (Au_1: Cu_3)-MOF/GCE samples, respectively) was added to BTC solution. The resulting mixture was crystallized in oven under 50 °C for 48 hours. Then, the MOF crystals was filtered with a 0.45 µm syringe filter (PVDF membrane, Sartorius, Germany). To obtain the oriented growth of the MOFs crystals, the prepared GCE was immersed in 10 ml of filtered MOFs solution. The carboxylic acid functionality emulates the organic linker BTC in the open framework structure [43]. The oriented growth of MOFs on GCE carried out in a glass closed reactor at room temperature for 10 hours.

2.2 Structural and electrochemical characterization of (Au_x: Cu_y)-MOFs/GCE

The morphology of synthesized (Au_x: Cu_y)-MOFs **(**x, y = 0, 1, 2 and 3) was analyzed by scanning electron microscopy (SEM, S360 Cambridge instrument, UK). The structural and crystallinity characteristics of modified electrodes were investigated with X-ray diffractometer (XRD, D8 Advance, Bruker, Germany) with Cu Kα radiation (λ = 1.5418 Å) operated at 40 kV and 30 mA.

Electrochemical studies were carried out in the three-electrode electrochemical cell which containing Ag/AgCl/(sat KCl) as reference electrode, a Pt wire as the counter electrode and (Au_x: Cu_y)-MOFs/GCE as the working electrode. Voltammetry and amperometry studies were performed with potentiostat (Autolab PGSTAT 302N, Metrohm, Autolab B.V., Utrecht, Netherlands) on the working electrodes in 0.1 M phosphate buffer solutions. The 0.1 M phosphate buffer solutions were prepared of H_3PO_4 (≥85%, Sigma-Aldrich, USA) and NaH_2PO_4 (>99%, Sigma-Aldrich, USA). The pH of phosphate buffer solutions was adjusted using a pH meter and the dropwise addition of both HCl and NaOH solutions.

3. RESULT AND DISCUSSION

3.1 Structural characterization of (Au_x: Cu_y)-MOFs

Figure 1 shows the SEM images of GCE and the prepared (Au_x: Cu_y)-MOFs/GCE. The (Au_x: Cu_y)-MOFs product indicated densely packed irregular nano-scale sheet-like MOFs. The surface of

sheets is smooth. Furthermore, highly porous spaces were observed in MOFs which increases the ability of the electrode to absorb.

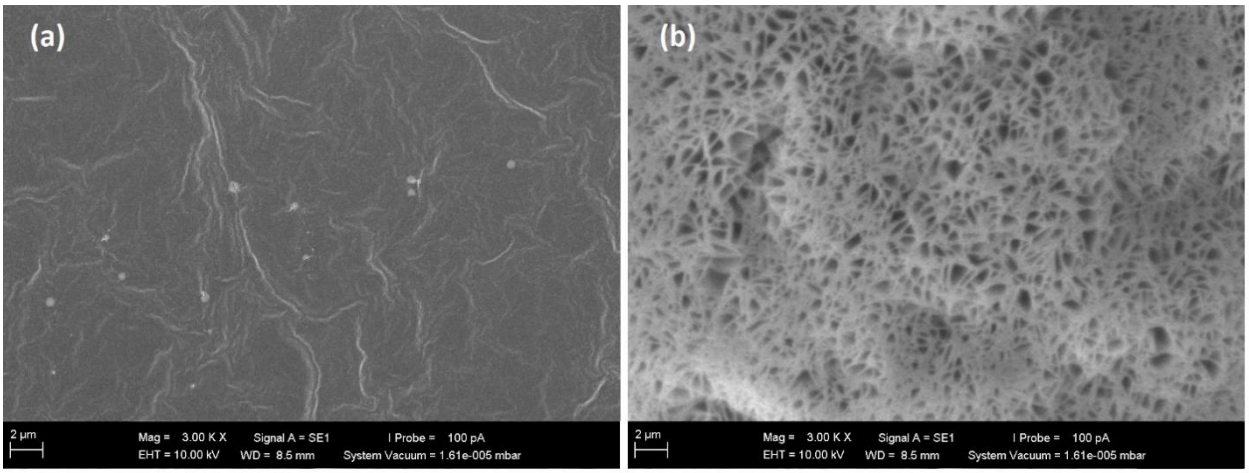

Figure 1. SEM image of (a) GCE and (b) (Au_x: Cu_y)-MOFs/GCE

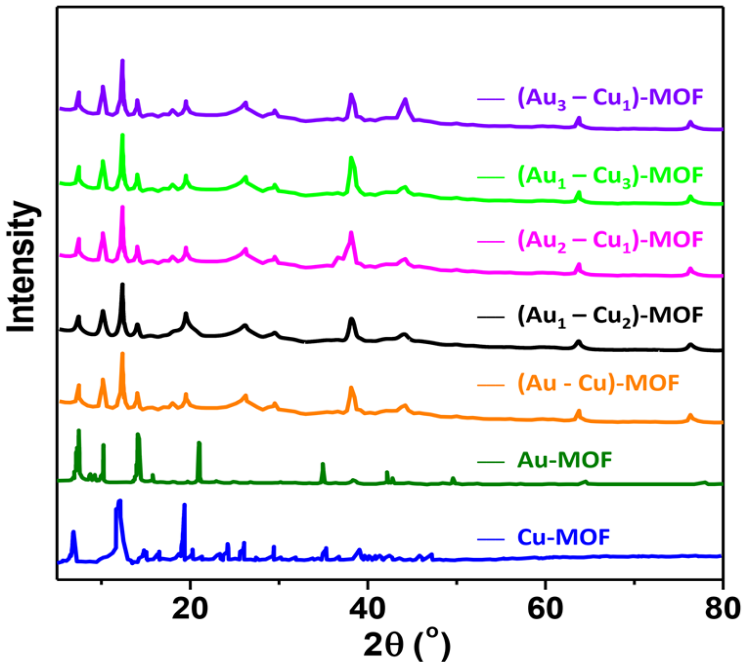

Figure 2. XRD pattern of (Au_x: Cu_y)-MOFs

Figure 2 shows the XRD patterns of the (Au_x: Cu_y)-MOFs. The highly crystallinity and the relative intensities of peaks are shown in XRD pattern of Cu-MOF that the typical peaks at $2\theta = 6.61^o$, 9.29^o, 11.18^o, 13.31^o, and 18.88^o correspond to (200), (220), (222), (400), and (440) planes, respectively are consistent with other reports of Cu-MOF synthesis [44, 45]. It can be seen that the high crystalline XRD pattern was recorded for Au-MOF. The main diffraction peak at $2\theta=38.31^o$ correspond to (111) was found for Au-MOF accordance with [46]. The XRD patterns of (Au: Cu)-MOF, (Au_1: Cu_2)-MOF, (Au_2: Cu_1)-MOF, (Au_1: Cu_3)-MOF, and (Au_3: Cu_1)-MOF show similar pattern with several main peaks

at 2θ = 38.49°, 44.55°, 64.77° and 77.79° which corresponding to (111), (200), (220), and (311) Au crystal planes, respectively.

3.2 Electrochemical studies of (Au_x: Cu_y)-MOFs/GCE to determination of H_2O_2

All cyclic voltammograms of electrodes were recorded in 0.1 M phosphate buffer solution pH 7.0 at a scan rate of 10 mV s^{-1} in the potential range of -1 to 1.0 V without any injection of H_2O_2. Figure 3a showed the recorded cyclic voltammograms of GCE, Cu-MOF/GCE, Au-MOF/GCE and (Au: Cu)-MOF/GCE. As seen, there are no redox peaks for GCE, corresponding with the inertia of carbon-based electrodes [47]. In Figure 3a, well defined redox peaks is displayed for Cu-MOF/GCE, Au-MOF/GCE and (Au: Cu)-MOF/GCE at 0.05 V and -0.22 V. For prepared Cu^- based MOFs, the redox peaks are caused by the conversion between Cu^{2+} and Cu^+ [47, 48]. At the reduction peak potential of about -0.22 V, Cu^{2+} is reduced to Cu^+, while at the oxidation peak potential of about 0.05 V, Cu^+ is oxidized to Cu^{2+} [47, 48]. Current of (Au: Cu)-MOF/GCE is more than the recorded cyclic voltammograms in Figure 3a. After the introduction of Au on Cu-MOF, the corresponding redox peak currents of Cu-MOF increases greatly, due to the excellent conductivity of Au that could accelerate the electron transfer [47]. Therefore, for optimization the Au/Cu volume ratio, the recorded cyclic voltammograms of (Au_1: Cu_2)-MOF/GCE, (Au_2: Cu_1)-MOF/GCE, (Au_1: Cu_3)-MOF/GCE, and (Au_3: Cu_1)-MOF/GCE are shown in Figure 3b. Comparison between the redox shows that (Au_1: Cu_2)-MOF/GCE displays high redox current.

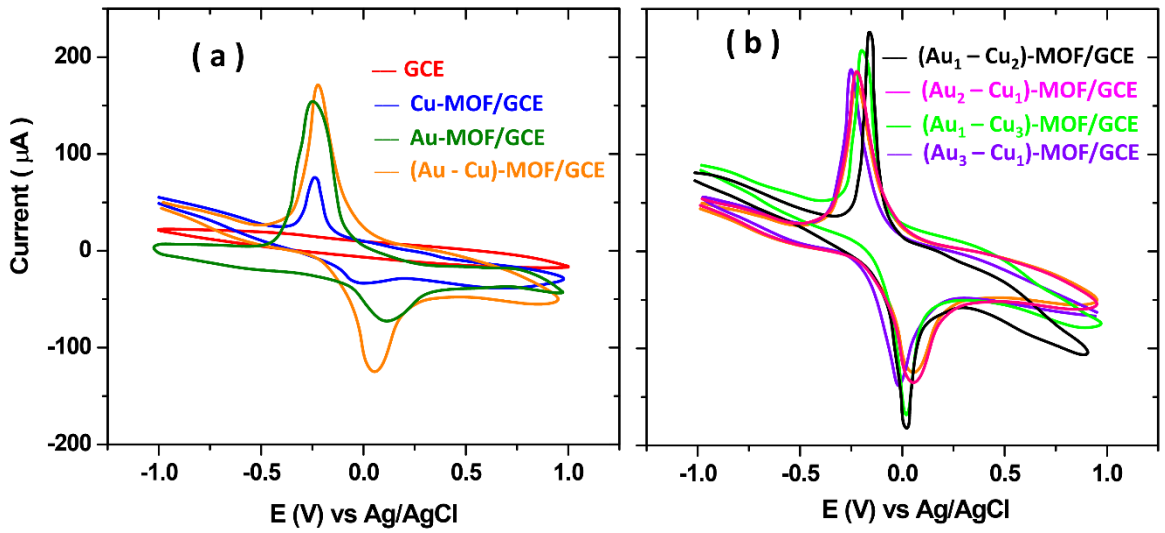

Figure 3. Recorded cyclic voltammograms of (Au_x: Cu_y)-MOFs/GCE in 0.1 M phosphate buffer solution pH 7.0 and the scan rate of 10 mV s^{-1}.

In order to investigate of the stability and response of prepared electrodes to injection of H_2O_2, the amperometrograms of electrodes were recorded in 0.1 M phosphate buffer solution at pH 7.0. Figure 4 shows the recorded amperometrograms of all electrodes before (first 100 s) and after of injection of 10 μM H_2O_2 solution (100 to 400 s). As shown in figure 4, the electro-catalytic currents were found for

GCE, Cu-MOF/GCE, Au-MOF/GCE, (Au: Cu)-MOF/GCE, (Au_1: Cu_2)-MOF/GCE, (Au_2: Cu_1)-MOF/GCE, (Au_1: Cu_3)-MOF/GCE, and (Au_3: Cu_1)-MOF/GCE of 10.01, 13.02, 13.83, 14.77, 19.10, 15.54, 16.26, and 15.84 µA, respectively. Furthermore, the electro-catalytic currents were changed for GCE, Cu-MOF/GCE, Au-MOF/GCE, (Au: Cu)-MOF/GCE, (Au_1: Cu_2)-MOF/GCE, (Au_2: Cu_1)-MOF/GCE, (Au_1: Cu_3)-MOF/GCE, and (Au_3: Cu_1)-MOF/GCE more than 71, 67, 45, 59, 6, 41, 17, and 57%, respectively. The recorded amperometrograms of (Au_2: Cu_1)-MOF/GCE and (Au_1: Cu_3)-MOF/GCE indicated more fast response toward other prepared electrodes. Thus, (Au_1: Cu_2)-MOF/GCE exhibits more electro-catalytic currents and more stability response to the injection of 1µM H_2O_2 solution. The excellent sensing properties of (Au_1: Cu_2)-MOF/GCE in the aqueous solution can be attributed to the high mechanical stability of Cu and high chemical stability of Au in MOF structure and the synergistic electro-catalytic effect of Cu-MOF and Au-MOF for determination of analyte [49]. Su et al. suggested the formation of hetero-interface between Au and Cu structures can facilitate charges separation and their migration, which would help to improve the catalytic activity of prepared electrode [50]. Moreover, porous structure of nano-sheets on electrode surface lead to the strong adsorption of MOFs on the GCE [51]. High sensitivity of electrode is related to high electrical conductivity of Cu [52], high aspect ratio and high active sites on the surface (Au_1: Cu_2)-MOF/GCE. The Au/Cu volume ratios of ½ might help to present concurrent properties Au (chemical stability) and Cu (high electrical conductivity). Thus, electrochemical reversibility and the high electron transfer rate of nanostructure surface of electrode illustrated the ability of (Au_1: Cu_2)-MOF/GCE to fast electron transferring between analyte and electrode surface in electro-catalysis process. Therefore, the (Au_1: Cu_2)-MOF/GCE was selected for further electrochemical study for the determination of H_2O_2 concentrations.

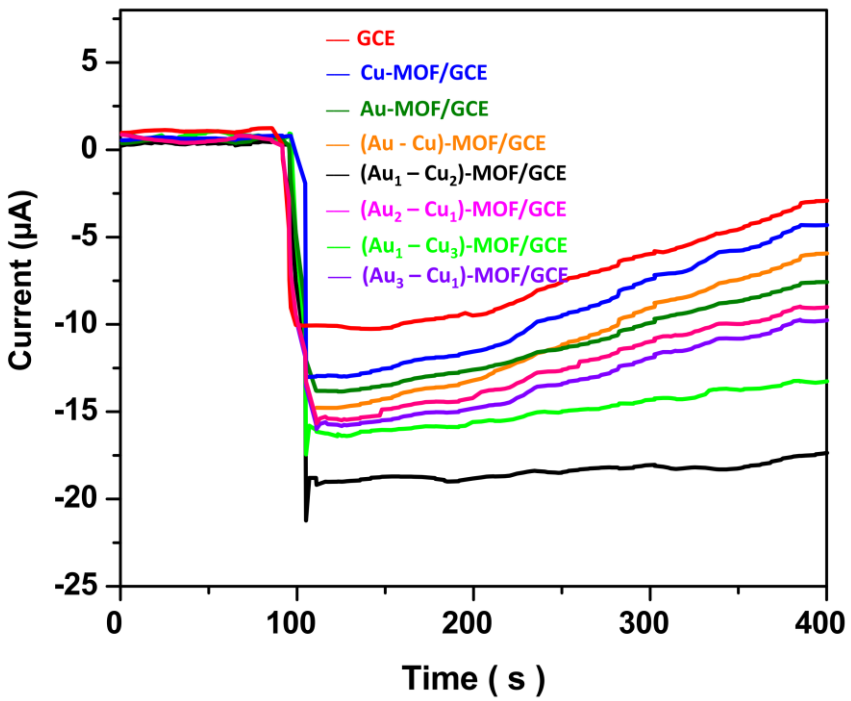

Figure 4. Recorded amperometrograms of (Au_x: Cu_y)-MOFs/GCE in 0.1 M phosphate buffer solution pH 7.0 at 0.05 V and rotation speed of 1000 rpm before and after of injection of 1 µM H_2O_2 solution.

In order to study the effect of H_2O_2 concentration, amperometry responses of (Au_1: Cu_2)-MOF/GCE were recorded under in successive injections of 1 µM H_2O_2 solution.

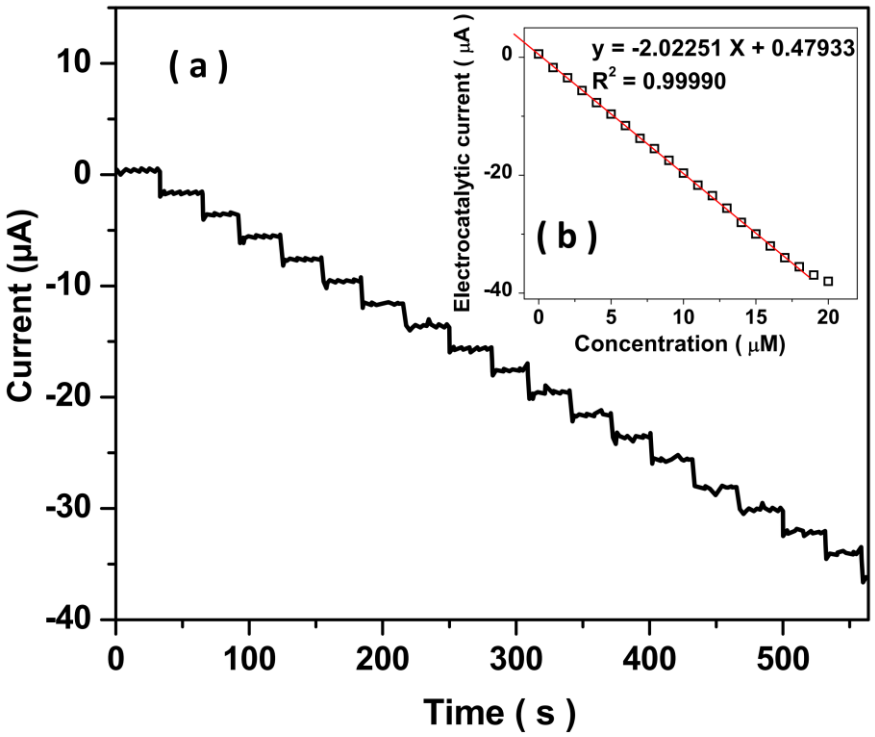

Figure 5. (a) The recorded amperometrogram of (Au_1: Cu_2)-MOF/GCE in 0.1 M phosphate buffer solution pH 7.0 at 0.05 V and rotation speed of 1000 rpm in successive additions of 1 µM H_2O_2 solution; (b) plot of calibration graph.

Table 1. Comparison of the analytical parameters of the different H_2O_2 sensor

Electrodes	**Technique**	**detection limit (µM)**	**Linear range (µM)**	**Sensitivity (µA/µM)**	**Ref.**
(Au_1: Cu_2)-MOF/GCE	Amperometry	0.014	1-19	2.022	This work
AuNPs-NH_2/Cu-MOF/GCE	Amperometry	1.2	5–850	1.71	[53]
PtAu/graphene-CNTs	Amperometry	0.6	2–8561	0.3134	[54]
Au nanochains and prussian blue nanorods @MWCNTs	Amperometry	0.5	1.75–1140	0.3	[55]
Cu/SiMO/MWCNT	Amperometry	6.53	6.53–5200	0.650	[56]
Cu-MOF/CPE	Amperometry	1.0	5–2800	-	[57]
zeolitic imidazolate - MOF /CNTs	Amperometry	0.62	2.5 –190	0.323	[58]
Cu–Ni$(OH)_2$/GCE	Cyclic voltammetry	1.5	5–140	0.408	[59]
Cu(II)- MOF/ CNTs	Cyclic voltammetry	0.46	3–70 and 70–30000	0.0366	[60]

Figure 5a shows the recorded amperometrograms with fast response to successive injections of H_2O_2 in electrochemical cell. The calibration graph in Figure 5b displays the equation current (µA) = -2.02251 [concentration of H_2O_2 (µM)] (µA/ µM) + 0.47933 (µA) with a correlation coefficient of 0.99990. In high injections of H_2O_2 (> 19 µM), the calibration graph exhibits deviations from linearity because of saturation of active site on electrode surface. Thus, the linear range, sensitivity and detection limit values were obtained 1 µM -19 µM, 2.022 µA/ µM and 0.014 µM, respectively.

The analytical parameters of the (Au_1: Cu_2)-MOF/GCE is compared with other H_2O_2 sensors as presented in Table 1. As shown, the H_2O_2 sensors with wide linear range have been reported. However, comparison with other nanomaterial based sensor, the (Au_1: Cu_2)-MOF/GCE indicates higher or comparative sensitivity due to the synergistic electro-catalytic activity of Cu and Au in determination of H_2O_2. When the results were compared to some noble metal-based hybrid composites such as Pt and Au metals [53-55], the (Au_1: Cu_2)-MOF/GCE electrode also shows lower cost benefits. The prepared bimetal-based MOF significantly increases the electro-catalytic active areas and promotes electron transfer in the reduction of H_2O_2.

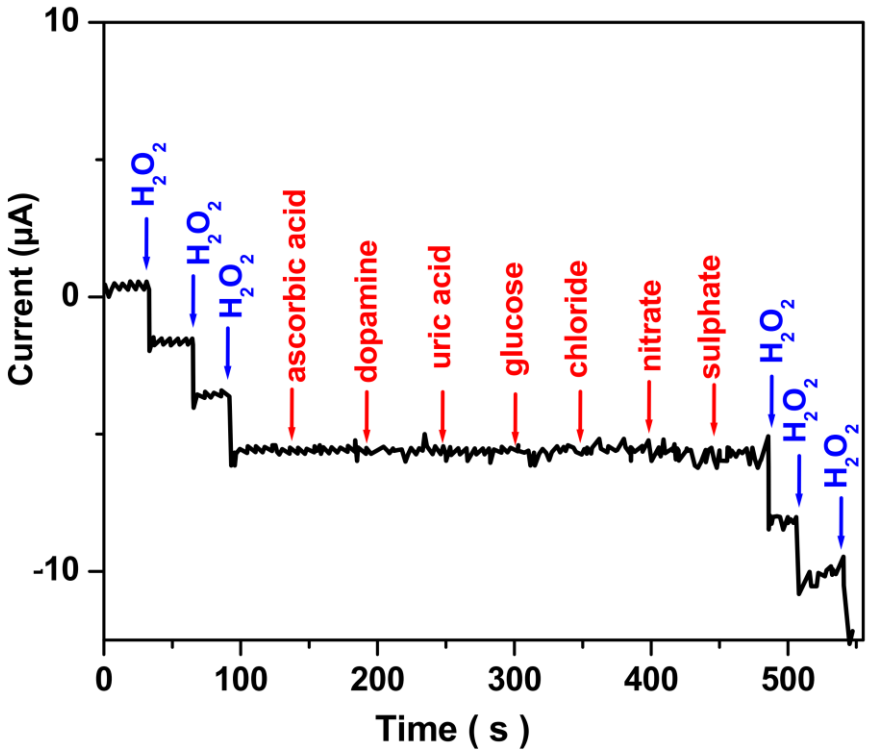

Figure 6. The recorded amperometrogram of (Au_1: Cu_2)-MOF/GCE electrode in 0.1 M phosphate buffer solution pH 7.0 at 0.05 V and rotation speed of 1000 rpm for 1 µM addition of H_2O_2 and 5 µM addition of ascorbic acid, dopamine, uric acid, glucose, chloride, nitrate and sulphate solutions.

Selectivity and interference response of (Au_1: Cu_2)-MOF/GCE was studied as H_2O_2 sensor. Therefore, the amperometry responses of prepared electrode were recorded in the presence different analytes. Figure 6 shows the recorded amperometrogram of (Au_1: Cu_2)-MOF/GCE in 0.1 M phosphate buffer solution at pH 7.0. As shown in figure 6, the electrode reveals a strong response to all additions of 1 µM H_2O_2 solution and does not display any significant response for the additions of 5 µM of ascorbic

acid, dopamine, uric acid, glucose, chloride, nitrate and sulphate. The results demonstrate that the modified electrode exhibits the selective response to H_2O_2 in present the above analytes and the above analytes do not interfere with detection of H_2O_2 on the surface of (Au_1: Cu_2)-MOF/GCE. The results were accordance with the Reddy et al. [61] and Liu et al. [62] findings for the determination of H_2O_2 using copper/copper oxide nanoparticles/pencil graphite lead electrode and copper nanoparticles on the polydopamine coated graphene oxide, respectively.

3.3 Detection of H_2O_2 in real water using (Au_1: Cu_2)-MOF/GCE

A real water sample was collected from Nanhu Lake (Jiaxing, China). The sample filtered using filter paper (11 µm, Whatman, UK) and was directly used for the preparation of 0.1 M phosphate buffer solution pH 7.0 without any further purification. The standard injection of H_2O_2 was applied for the determination of H_2O_2 in the sample. Figure 7a shows the recorded amperometrogram of (Au_1: Cu_2)-MOF/GCE in prepared real sample in successive injections of 1 µM H_2O_2 solution. Figure 7b displays the calibration graph as current (µA) = -2.034 [concentration of H_2O_2 (µM)] (µA/ µM) + 0.0479 (µA) with a correlation coefficient of 0.9997. Thus, the concentration of H_2O_2 was evaluated 0.023 ± 0.004 µM in 0.1 M phosphate buffer solution. The recovery and relative standard deviation (RSD) values of the sample is presented in Table 2. As shown, satisfactory RSD and recovery values are less than 4.51% and more than 91.86%, respectively. The results illustrate that (Au_1: Cu_2)-MOF/GCE can be considered as H_2O_2 sensor in real samples.

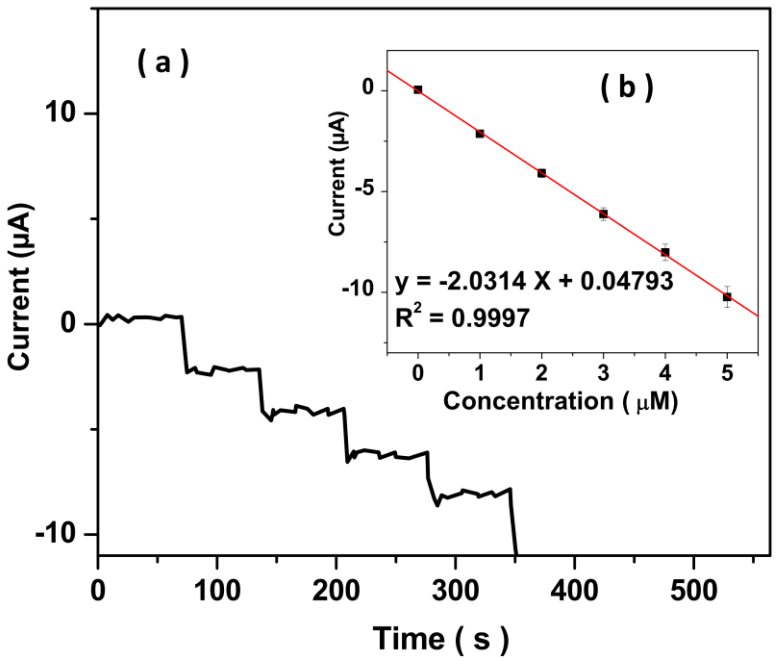

Figure 7. (a) The recorded amperometrogram of (Au_1: Cu_2)-MOF/GCE in 0.1 M phosphate buffer solution pH 7.0 at 0.05 V and rotation speed of 1000 rpm in addition of 1 µM H_2O_2 in a real sample; (b) Plot of calibration graph.

Table 2. Results of determination of H_2O_2 in real water using (Au_1: Cu_2)-MOF/GCE.

Lake water sample	Added (μM)	Measured (μM)	RSD (%)*	Recovery (%)
1	1.00	0.94	2.89	94.00
2	2.00	1.88	2.95	94.00
3	3.00	2.91	3.10	97.00
4	4.00	3.93	3.57	98.25
5	5.00	4.91	4.51	98.20

*RSD values was obtained from four independent measurements.

4. CONCLUSION

The Electrochemical characterization of (Au_x: Cu_y)-MOFs/GCE as H_2O_2 sensor was carried out by cyclic voltammetry and amperometry methods. The (Au_x: Cu_y)-MOFs were synthesized through the oriented growth technique and were applied for the modification of GCE. The structure, morphology and crystallinity of synthesized (Au_x: Cu_y)-MOFs were investigated by SEM and XRD analyses. Results displayed high crystalline, porous and densely packed irregular nano-sheet structures of (Au_x: Cu_y)-MOFs were prepared on GCE. The electrochemical studies showed that (Au_2: Cu_1)-MOF/GCE reveals fast response, more electro-catalytic currents and more stability response to the injection of H_2O_2 solution toward other prepared electrodes. The wide linear range, sensitivity and detection limit of sensor were estimated 1 to 19 μM, 2.022 μA/μM and 0.014 μM, respectively. Comparison of (Au_1:Cu_2)-MOF/GCE performance with other nanomaterial based sensor exhibits higher or comparative sensitivity because of the synergistic electro-catalytic activity of Cu and Au in the determination of H_2O_2. Study of selectivity and interference response of (Au_1:Cu_2)-MOF/GCE indicated that the modified electrode exhibits the selective response to H_2O_2 and the ascorbic acid, dopamine, uric acid, glucose, chloride, nitrate and sulphate analytes do not interfere with the detection of H_2O_2 on the surface of (Au_1:Cu_2)-MOF/GCE. Further study of the modified electrode on water of Nanhu Lake as real sample showed satisfactory RSD and recovery values was less than 4.51% and more than 91.86%, respectively. The results show that (Au_1:Cu_2)-MOF/GCE has potential as H_2O_2 sensor in practical applications.

ACKNOWLEDGEMENT
This research was sponsored by Natural Science Foundation of Heilongjiang Province, Design, synthesis and properties of fluorescent crystalline complexes based on polyoxometalates and nontoxic MOFs, QC2017004 and Science Foundation of Daqing Normal University, Design, synthesis and transmission of polyoxometalates drugs based on biological MOFs carriers, 19ZR03.

References

1. D. E Edmondson, *Current Pharmaceutical Design*, 20 (2014) 155.
2. M. Hoshino, S. Kamino, M. Doi, S. Takada, S. Mitani, R. Yanagihara, M. Asano, T. Yamaguchi and Y. Fujita, *Spectrochimica acta part A: molecular and Biomolecular spectroscopy*, 117 (2014) 814.
3. H. Karimi-Maleh and O.A. Arotiba, *Journal of colloid and interface science*, 560 (2020) 208.

4. J. Rouhi, S. Mahmud, S. Hutagalung and S. Kakooei, *Micro & Nano Letters*, 7 (2012) 325.
5. V. Lobo, A. Patil, A. Phatak and N. Chandra, *Pharmacognosy reviews*, 4 (2010) 118.
6. L.A. Hadwiger and K. Tanaka, *Frontiers in Plant Science*, 8 (2017) 446.
7. M.B. Grisham, *Comparative Biochemistry and Physiology Part A: Molecular & Integrative Physiology*, 165 (2013) 429.
8. H. Karimi-Maleh, F. Karimi, M. Alizadeh and A.L. Sanati, *The Chemical Record*, 20 (2020) 682.
9. Z. Shamsadin-Azad, M.A. Taher, S. Cheraghi and H. Karimi-Maleh, *Journal of Food Measurement and Characterization*, 13 (2019) 1781.
10. Y. Ding, H. Liu, L.-N. Gao, M. Fu, X. Luo, X. Zhang, Q. Liu and R.-C. Zeng, *Journal of Alloys and Compounds*, 785 (2019) 1189.
11. R.C. Castro, J.X. Soares, D.S. Ribeiro and J.L. Santos, *Sensors and Actuators B: Chemical*, 296 (2019) 126665.
12. D. Mukhopadhyay, P. Dasgupta, D.S. Roy, S. Palchoudhuri, I. Chatterjee, S. Ali and S.G. Dastidar, *Free Radicals & Antioxidants*, 6 (2016) 1.
13. M. Song, J. Wang, B. Chen and L. Wang, *Analytical chemistry*, 89 (2017) 11537.
14. D. Sodzel, V. Khranovskyy, V. Beni, A.P. Turner, R. Viter, M.O. Eriksson, P.-O. Holtz, J.-M. Janot, M. Bechelany and S. Balme, *Microchimica Acta*, 182 (2015) 1819.
15. F.J. Perez and S. Rubio, *Plant Growth Regulation*, 48 (2006) 89.
16. A. Brestovisky, E. KirowaEisner and J. Osteryoung, *Analytical Chemistry*, 55 (1983) 2063.
17. H. Razmi and A. Taghvimi, *International Journal of Electrochemical Science*, 5 (2010) 751.
18. A. Babaei, D.J. Garrett and A.J. Downard, *International Journal of Electrochemical Science*, 7 (2012) 3141.
19. F. Tahernejad-Javazmi, M. Shabani-Nooshabadi and H. Karimi-Maleh, *Composites Part B: Engineering*, 172 (2019) 666.
20. B. Liu and M. Wang, *International Journal of Electrochemical Science*, 8 (2013) 8572.
21. Z. Savari, S. Soltanian, A. Noorbakhsh, A. Salimi, M. Najafi and P. Servati, *Sensors and Actuators B: Chemical*, 176 (2013) 335.
22. H. Karimi-Maleh, K. Cellat, K. Arıkan, A. Savk, F. Karimi and F. Şen, *Materials Chemistry and Physics*, 250 (2020) 123042.
23. M. Negahdary, A. Asadi, S. Mehrtashfar, M. Imandar, H. Akbari-Dastjerdi, F. Salahi, A. Jamaleddini and M. Ajdary, *International Journal of Electrochemical Science*, 7 (2012) 5185.
24. C.X. Lei, H. Wang, G.L. Shen and R.Q. Yu, *Electroanalysis: An International Journal Devoted to Fundamental and Practical Aspects of Electroanalysis*, 16 (2004) 736.
25. A. Khodadadi, E. Faghih-Mirzaei, H. Karimi-Maleh, A. Abbaspourrad, S. Agarwal and V.K. Gupta, *Sensors and actuators b: chemical*, 284 (2019) 568.
26. R. Dalvand, S. Mahmud and J. Rouhi, *Materials Letters*, 160 (2015) 444.
27. R. Savari, H. Savaloni, S. Abbasi and F. Placido, *Sensors and Actuators B: Chemical*, 266 (2018) 620.
28. F. Chahshouri, H. Savaloni, E. Khani and R. Savari, *Journal of Micromechanics and Microengineering*, 30 (2020) 075001.
29. V. Mani, S.-M. Chen, K. Raj and M. Kesavan, *International Journal of Electrochemical Science*, 11 (2016) 2954.
30. M. Naseri, L. Fotouhi and A. Ehsani, *J. Electrochem. Sci. Technol*, 9 (2018) 28.
31. W.-X. Zhang, P.-Q. Liao, R.-B. Lin, Y.-S. Wei, M.-H. Zeng and X.-M. Chen, *Coordination Chemistry Reviews*, 293 (2015) 263.
32. M. Miraki, H. Karimi-Maleh, M.A. Taher, S. Cheraghi, F. Karimi, S. Agarwal and V.K. Gupta, *Journal of Molecular Liquids*, 278 (2019) 672.
33. N. Naderi, M. Hashim and J. Rouhi, *International Journal of Electrochemical Science*, 7 (2012) 8481.

34. M. Joharian, A. Morsali, A.A. Tehrani, L. Carlucci and D.M. Proserpio, *Green chemistry*, 20 (2018) 5336.
35. J. Rouhi, C.R. Ooi, S. Mahmud and M.R. Mahmood, *Electronic Materials Letters*, 11 (2015) 957.
36. X. Wang, J. Zhang, Y. Wei, T. Xing, T. Cao, S. Wu and F. Zhu, *Analyst*, 145 (2020) 1933.
37. H. Wu, M. Li, Z. Wang, H. Yu, J. Han, G. Xie and S. Chen, *Analytica Chimica Acta*, 1049 (2019) 74.
38. J. Rouhi, S. Kakooei, S.M. Sadeghzadeh, O. Rouhi and R. Karimzadeh, *Journal of Solid State Electrochemistry*, 24 (2020)
39. W.-J. Shen, Y. Zhuo, Y.-Q. Chai and R. Yuan, *Analytical chemistry*, 87 (2015) 11345.
40. Y. Zhang, J. Song, Q. Pan, X. Zhang, W. Shao, X. Zhang, C. Quan and J. Li, *Journal of Materials Chemistry B*, 8 (2020) 114.
41. H. Karimi-Maleh, M. Sheikhshoaie, I. Sheikhshoaie, M. Ranjbar, J. Alizadeh, N.W. Maxakato and A. Abbaspourrad, *New Journal of Chemistry*, 43 (2019) 2362.
42. Y. Zhou, C. Li, Y. Hao, B. Ye and M. Xu, *Talanta*, 188 (2018) 282.
43. E. Biemmi, C. Scherb and T. Bein, *Journal of the American Chemical Society*, 129 (2007) 8054.
44. X. Mu, Y. Chen, E. Lester and T. Wu, *Microporous and Mesoporous Materials*, 270 (2018) 249.
45. T. Noor, M. Ammad, N. Zaman, N. Iqbal, L. Yaqoob and H. Nasir, *Catalysis Letters*, 149 (2019) 3312.
46. A. Corma, M. Iglesias, F.X.L. i Xamena and F. Sánchez, *Chemistry–A European Journal*, 16 (2010) 9789.
47. H. Chen, T. Yang, F. Liu and W. Li, *Sensors and Actuators B: Chemical*, 286 (2019) 401.
48. Q. Zhang and Y. Hua, *Physical Chemistry Chemical Physics*, 16 (2014) 27088.
49. Y. Liu, L. Huang, X. Zhu, Y. Fang and S. Dong, *Nanoscale*, 12 (2020) 1811.
50. Y. Su, H. Guo, Z. Wang, Y. Long, W. Li and Y. Tu, *Sensors and Actuators B: Chemical*, 255 (2018) 2510.
51. X. Zhang, A. Wu, X. Wang, C. Tian, R. An and H. Fu, *Journal of Materials Chemistry A*, 6 (2018) 17905.
52. L. Yang, N. Huang, L. Huang, M. Liu, H. Li, Y. Zhang and S. Yao, *Analytical Methods*, 9 (2017) 618.
53. W. Dang, Y. Sun, H. Jiao, L. Xu and M. Lin, *Journal of Electroanalytical Chemistry*, 856 (2020) 113592.
54. D. Lu, Y. Zhang, S. Lin, L. Wang and C. Wang, *Talanta*, 112 (2013) 111.
55. S. Chen, L. Ma, R. Yuan, Y. Chai, Y. Xiang and C. Wang, *European Food Research and Technology*, 232 (2011) 87.
56. K.-C. Lin, Y.-H. Chen and S.-M. Chen, *Int. J. Electrochem. Sci*, 10 (2015) 9205.
57. D. Zhang, J. Zhang, R. Zhang, H. Shi, Y. Guo, X. Guo, S. Li and B. Yuan, *Talanta*, 144 (2015) 1176.
58. Y. Fu, J. Dai, Y. Ge, Y. Zhang, H. Ke and W. Zhang, *Molecules*, 23 (2018) 2552.
59. A. Gu, G. Wang, J. Gu, X. Zhang and B. Fang, *Electrochimica acta*, 55 (2010) 7182.
60. E. Zhou, Y. Zhang, Y. Li and X. He, *Electroanalysis*, 26 (2014) 2526.
61. G.R.K. Reddy, M. Hyder and P.S. Kumar, *Materials Today: Proceedings*, 4 (2017) 12457.
62. Y. Liu, Y. Han, R. Chen, H. Zhang, S. Liu and F. Liang, *PLoS One*, 11 (2016) e0157926.